Research Square

Preprints are preliminary reports that have not undergone peer review.
They should not be considered conclusive, used to inform clinical practice,
or referenced by the media as validated information.

Characterization of N-Glycosylation Remodeling in Cerebrospinal Fluid Extracellular Vesicles in Children with Purulent Meningitis and Viral Meningitis: An Exploratory Glycomics Study Based on MALDI-TOF/TOF-MS

YUJIA RUAN
Hubei University of Chinese Medicine
Yinfeng Shen
dfydzsjd@126.com
Hubei University of Chinese Medicine

Research Article

Keywords: Cerebrospinal Fluid, N-Glycosylation, Extracellular Vesicles, Purulent Meningitis, Viral Meningitis

Posted Date: September 7th, 2026

DOI: https://doi.org/10.21203/rs.3.rs-10767266/v1

License: This work is licensed under a Creative Commons Attribution 4.0 International License.
Read Full License

Additional Declarations: No competing interests reported.

Version of Record: A version of this preprint was published at Glycoconjugate Journal on November 7th, 2026. See the published version at https://doi.org/10.1007/s10719-026-10232-2.

Characterization of N-Glycosylation Remodeling in Cerebrospinal Fluid Extracellular Vesicles in Children with Purulent Meningitis and Viral Meningitis: An Exploratory Glycomics Study Based on MALDI-TOF/TOF-MS

Yujia Ruan[1], Yinfeng Shen[2345]*

Abstract

To investigate differences in cerebrospinal fluid (CSF) N-glycosylation profiles among children with purulent meningitis (PM), viral meningitis (VM), and disease controls (DC). This retrospective exploratory study included six children with PM, three with VM, and three children with leukemia in complete remission without central nervous system infection. CSF-derived extracellular vesicles（CSF-EVs）were characterized by transmission electron microscopy, nanoparticle tracking analysis, and Western blotting. N-glycans were released using PNGase F, purified by porous graphitized carbon solid-phase extraction, and analyzed by matrix-assisted laser desorption/ionization time-of-flight mass spectrometry. Fifteen derived glycan traits were quantified. Group differences were assessed using Kruskal–Wallis tests with pairwise comparisons, and associations with clinical inflammatory markers were evaluated using Spearman correlation.CSF N-glycan profiles showed distinct patterns across the three groups. Hierarchical clustering based on glycan traits separated PM, VM, and DC samples. Compared with DC, both PM and VM showed altered sialylation, but their remodeling patterns differed. PM showed increased highly sialylated glycan traits, whereas VM showed increased disialylation and reduced galactosylation- and core fucosylation-associated traits. Bisecting GlcNAc-related traits were reduced in both infection groups. Total bisecting GlcNAc（B Total）was positively correlated with serum procalcitonin (PCT) levels (r=0.681, P=0.015). Pediatric CNS infections were associated with distinct CSF N-glycan remodeling patterns. These findings provide preliminary evidence of infection-associated glycomic alterations and support further validation in larger cohorts.

Keywords Cerebrospinal Fluid; N-Glycosylation; Extracellular Vesicles; Purulent Meningitis; Viral Meningitis

Introduction

Purulent meningitis (PM) and viral meningitis (VM) are two of the most common central nervous system

[1] Hubei Provincial Hospital of TCM, Hubei University of Chinese Medicine, Wuhan, Hubei 430065, China

[2] Corresponding author: Yinfeng Shen, Email: dfydzsjd@126.com

[3] Hubei Provincial Hospital of Traditional Chinese Medicine, Affiliated with Hubei University of Chinese Medicine, Wuhan, Hubei 430061, China;Email: dfydzsjd@126.com

[4] Hubei Shizhen Laboratory, Wuhan, Hubei 430065, China

[5] Hubei Provincial Key Laboratory of Research and Application of Liver and Kidney in Traditional Chinese Medicine, Wuhan, Hubei 430065, China

infections in children. Purulent meningitis, also referred to as bacterial meningitis, is one of the top ten causes of death in children under 5 years of age, with a case-fatality rate of up to 30%. Neurological complications, including hearing loss, developmental delay, and motor impairment, may occur in 50% of children with purulent meningitis; however, timely administration of antibiotics can significantly improve clinical outcomes[1-2]. In contrast, VM is primarily managed with symptomatic and supportive treatment. Therefore, rapid diagnosis may help reduce hospitalization rates, length of hospital stay, and healthcare costs in patients with VM, while preventing unnecessary antibiotic use and the subsequent development of antimicrobial resistance, thereby minimizing adverse effects on patients[3-4]. Serum procalcitonin (PCT), a sensitive biomarker reflecting the burden of systemic bacterial infection and the severity of the inflammatory response, has been widely used as an adjunctive marker for differentiating bacterial from viral infections in children[5-8]. However, the nonspecific clinical manifestations of central nervous system infections in the early stages of disease make timely differentiation between PM and VM a major clinical challenge[9-13].

In recent years, research on exosomes has provided new perspectives for disease diagnosis and treatment[10-12]. Exosomes are extracellular vesicles measuring approximately 20–150 nm that are released by most cell types into body fluids, including blood, urine, cerebrospinal fluid, saliva, and amniotic fluid. They carry various biomolecules, such as proteins, microRNAs, and lipids, and participate in intercellular communication and pathological processes[10,13-14]. In cerebrospinal fluid (CSF), exosomes contain proteins derived from neurons, oligodendrocytes, astrocytes, and microglia, which are involved in nervous system development and various physiological and pathological processes[14]. Recent studies have shown that, in addition to proteins and lipids, extracellular vesicles (EVs) also display diverse glycoconjugates on their surfaces, including O-glycans, N-glycans, and glycosphingolipids such as gangliosides, as well as various glycosylation modifications[15-17]. EV glycosylation plays critical roles in various disease processes, including cell–cell and cell–substrate interactions, bacterial adhesion, cellular immunogenicity, and signal transduction[15-18].

N-glycosylation is the process by which oligosaccharides are attached to the amide nitrogen of an asparagine (Asn) residue[19]. This process is initiated in the endoplasmic reticulum (ER) and completed in the Golgi apparatus. As a common form of protein glycosylation, N-glycosylation not only affects protein structure and function but also plays a critical role in regulating intercellular interactions and signal transduction and is closely associated with disease progression. Alterations in N-glycosylation have been observed in numerous inflammatory diseases. Proinflammatory cytokines can regulate cell-surface glycosylation by modulating the expression of glycosyltransferases and sulfotransferases involved in glycan biosynthesis, thereby inducing the expression of specific carbohydrate antigens on the cell surface. These antigens can be recognized by different types of lectins or bacterial adhesins, thereby promoting disease progression. Modulation of glycosylation levels may exacerbate or attenuate inflammatory responses. Such alterations may affect cellular signaling pathways, particularly the

activities of the NF-κB and MAPK signaling pathways, thereby regulating the magnitude and persistence of inflammation[20-21]. Glycosylation can also modulate the biological functions of immune cells by promoting leukocyte recruitment to sites of inflammation and may exert either pro-inflammatory or anti-inflammatory effects. The mechanisms underlying the interactions between protein glycosylation and systemic inflammatory responses, autoimmune responses, and tumorigenesis have not yet been fully elucidated and remain an active area of investigation. To date, alterations in CSF N-glycosylation profiles have been reported in adults with neurological disorders[22-23]. However, no studies have yet investigated alterations in N-glycosylation in the CSF or CSF-derived extracellular vesicles of children with PM or VM. Therefore, further investigation of N-glycosylation alterations in the CSF of children may not only improve our understanding of the mechanisms underlying the development of pediatric central nervous system infections but also reveal novel disease biomarkers for the early differentiation of purulent meningitis from viral meningitis.

The present study aimed to systematically characterize N-glycosylation profiles in CSF-derived extracellular vesicles (CSF-EVs) from children with purulent meningitis and viral meningitis, investigate patterns of CSF-EV N-glycosylation remodeling across different infectious states, and evaluate the associations between derived glycan traits and clinical inflammatory markers. CSF and CSF-derived extracellular vesicles were isolated from pediatric patients, and modern analytical techniques, including matrix-assisted laser desorption/ionization time-of-flight mass spectrometry (MALDI-TOF-MS), were employed to characterize the N-glycosylation profiles of EV-associated proteins. This study may not only facilitate the identification of candidate glycomic biomarkers associated with purulent meningitis and viral meningitis in children but also provide preliminary evidence for the future development of differential diagnostic approaches for pediatric purulent meningitis and viral meningitis.

Study Design and Participants

This case–control study was conducted at Wuhan Children's Hospital, where CSF samples were collected from pediatric participants. The study population was divided into three groups: a disease control group (DC), a purulent meningitis group (PM), and a viral meningitis group (VM). The DC group comprised children with acute leukemia in complete remission. None had fever, headache, seizures, or other symptoms suggestive of central nervous system infection, and routine CSF, biochemical, and pathogen testing showed no evidence of CNS infection. CSF samples were obtained from residual specimens collected during routine lumbar puncture performed for disease management or treatment-response assessment.PM was diagnosed based on clinical manifestations, CSF findings, and microbiological evidence, including positive CSF culture, positive pathogen nucleic acid testing, or fulfillment of established diagnostic criteria for bacterial meningitis. VM was diagnosed based on meningeal signs, neurological symptoms, inflammatory CSF findings, and positive viral nucleic acid or serological testing,

or according to established clinical diagnostic criteria.Exclusion criteria included concomitant severe infectious diseases, genetic or metabolic disorders, autoimmune diseases, pre-existing neurological disorders, and insufficient sample volume or inadequate sample quality for analysis.

Materials and Methods

Cerebrospinal Fluid Collection and Extracellular Vesicle Isolation

Cerebrospinal fluid (CSF) samples were collected by standard lumbar puncture. For each participant, 3–5 mL of CSF was collected, with a portion used for routine clinical testing and the remainder for glycomics analysis. Samples were immediately placed on ice after collection, and pretreatment was completed within 1 h. Samples were centrifuged at 3,000 × g for 15 min at 4 °C, after which the supernatants were transferred to new cryovials, aliquoted, and stored at −80 °C.

Extracellular Vesicle Isolation

CSF specimens thawed at room temperature were centrifuged at 10,000 × g for 30 min at 4 °C to remove cellular debris. The samples were then subjected to ultracentrifugation at 140,000 × g for 70 min at 4 °C using an XPN100 ultracentrifuge (Beckman Coulter). Following ultracentrifugation, the supernatant was carefully removed, and the pellet was resuspended in phosphate-buffered saline (PBS), thoroughly homogenized by vortexing, and subjected to a second ultracentrifugation at 140,000 × g for 70 min at 4 °C. The resulting pellet was collected as the extracellular vesicle fraction.

CSF samples from all participants underwent extracellular vesicle isolation independently according to the above procedure. N-glycan release and MALDI-TOF-MS analysis were subsequently performed separately for each individual sample without pooling within groups, thereby ensuring traceability of glycomic data at the individual level for subsequent between-group and correlation analyses.

Transmission Electron Microscopy

To verify that the isolated particles met the criteria of the International Society for Extracellular Vesicles (ISEV)[12], the morphology, particle size distribution, and marker proteins of CSF-derived extracellular vesicles (CSF-EVs) were characterized. Following isolation, the morphology of the extracellular vesicles was examined by transmission electron microscopy (TEM). The extracellular vesicles were resuspended in PBS and fixed for 15 min using 40 g/L paraformaldehyde and an equal volume of 1% glutaraldehyde. The extracellular vesicle suspension was then applied to 400-mesh carbon-coated copper grids (Ted Pella Inc., Redding, CA, USA) and allowed to dry at room temperature for 10 min. The grids were stained with uranyl oxalate solution at pH 7.0 for 10 min, followed by staining with methylcellulose–uranyl acetate solution at pH 4.0 for 10 min. The latter solution consisted of 9 parts of 2% methylcellulose and

1 part of 4% uranyl acetate. After staining, the samples were dried at room temperature for 10 min and examined using a JEM-1400 Plus transmission electron microscope (JEOL Ltd., Tokyo, Japan).

Nanoparticle Tracking Analysis

The particle size distribution and concentration of CSF-derived extracellular vesicles (CSF-EVs) were determined by nanoparticle tracking analysis (NTA) using a ZetaView Particle Metrix system (PMX-120, Particle Metrix, Germany). Before analysis, the instrument was calibrated using 100-nm polystyrene standard microspheres (Thermo Fisher Scientific, USA). For each sample, videos were acquired and analyzed using the NTA software to determine particle size distribution and concentration (particles/mL). Data from all samples were analyzed using the software's built-in batch-processing program.

Western Blot Analysis of Extracellular Vesicle Marker Proteins

The protein concentrations of CSF-EVs were determined using a BCA assay kit (Beyotime, China) according to the manufacturer’s instructions. CSF-EVs were lysed with ice-cold RIPA lysis buffer (Beyotime, China) containing a protease inhibitor cocktail (Sigma, USA). Lysates in equal amounts of proteins were separated by SDS-PAGE (Bio-Rad, USA) and then transferred to PVDF membranes (Pall Corporation, USA). After rinsing with TBS (Signalway Antibody, USA) several times and blocking with 5% non-fat milk (BBI, China), the membranes were incubated with anti-CD9 primary antibody (DLM, DL210002, China), anti-Calnexin primary antibody (Proteintech, 10427-2-AP, USA), anti-CD81 primary antibody (Proteintech, 66866-1-Ig, USA) and anti-TSG101 primary antibody (DLM, DL210005, China) overnight. Followed by thoroughly washing, HRP-conjugated secondary antibodies (Proteintech, SA00001-1, America) were incubated with membranes in darkness for 1 h. ECL reagent (Tanon, China) was added to the membranes to visualize the immunoreactive protein bands, and the ChemiDoc MP imaging system (Bio-Rad, USA) was used to analysis.

Enzymatic Release and Preparation of N-Glycans from CSF-EVs Glycoproteins

CSF-EV samples obtained by ultracentrifugation as described above, containing 20 μg of total protein, were accurately measured. Dithiothreitol (DTT) was added sequentially to reduce disulfide bonds, followed by iodoacetamide for cysteine alkylation. The denatured proteins were then immobilized in situ onto pre-wetted PVDF membranes and stained with Direct Blue. The target protein spots were excised and subjected to in-membrane enzymatic digestion. Mass spectrometry-grade recombinant PNGase F (2 U) was added to the reaction system, and enzymatic digestion was performed continuously at 37 °C for 16 h to quantitatively release N-glycans linked to asparagine (Asn) residues.

The released free N-glycans were subjected to ammonium acetate hydroxylation treatment and subsequently reduced with sodium borohydride (NaBH4) at 50 °C for 3 h to stabilize the reducing termini of the glycans. The reaction was terminated by the addition of glacial acetic acid. The reaction products

were sequentially passed through strong cation-exchange (SCX) resin microcolumns and porous graphitized carbon (PGC) solid-phase extraction (SPE) microcolumns for dual-stage desalting and matrix purification. The eluates were collected and dried for subsequent analysis.

MALDI-TOF/TOF Mass Spectrometric Analysis and Glycan Annotation

Purified N-glycan fractions were analyzed using a MALDI-TOF/TOF mass spectrometer (Applied Biosystems 4700 Proteomics Analyzer, Framingham, MA, USA). Dried glycan samples were reconstituted in 50% (v/v) acetonitrile, mixed with 2,5-dihydroxybenzoic acid (DHB) matrix, and spotted onto a stainless-steel MALDI target plate. After air-drying and co-crystallization, spectra were acquired in positive-ion reflector mode over an *m/z* range of approximately 1,000–5,000. Multiple laser positions were sampled for each spot, and the resulting spectra were accumulated to obtain a representative spectrum. External calibration, baseline correction, noise filtering, peak detection, and centroiding were performed using consistent parameters across all samples.[24-26].

Individual glycan signals were assigned according to their observed m/z values and corresponding theoretical N-glycan compositions, taking into account relevant sodium adducts. Glycan assignments were evaluated based on mass accuracy, isotopic patterns, and previously reported N-glycan compositions. The assigned glycan compositions were cross-referenced with previously reported N-glycan compositions and entries available in the GlycoStore database. The detected glycan peaks were subsequently classified according to major structural features, including high-mannose, hybrid, complex, fucosylated, sialylated, and bisected structures. Each reproducibly detected glycan was assigned a unique peak identifier (Peak 1–54). For comparative analysis, the intensity of each annotated glycan was normalized to the total intensity of all annotated glycan peaks detected in the corresponding spectrum, yielding the relative abundance of individual N-glycans. These data were subsequently used to calculate glycan-derived traits according to predefined structural categories, with the detailed peak-to-trait assignments provided in Supplementary Table **S1**.

Data Analysis

Data preprocessing, normalization, and integration were performed using internally developed MATLAB R2014b functions and Perl scripts. All statistical analyses were conducted using RStudio, SPSS, Perseus v1.6.10.43, and GraphPad Prism 9 (Dotmatics, MA, USA). The normality of continuous variables was initially assessed using the Shapiro–Wilk test. Normally distributed data were compared using one-way analysis of variance (ANOVA), whereas non-normally distributed data were compared using the Kruskal–Wallis test.

Between-group comparisons of the 15 derived glycan traits were reported using unadjusted nominal P values. A $P < 0.05$ was considered statistically significant, whereas results with P values between 0.05 and 0.10 were considered indicative of a potential trend and were not interpreted as confirmatory findings

but rather as hypothesis-generating observations for subsequent validation in larger cohorts. For multiple comparisons involving individual glycan peaks (Peak 1–54) during exploratory differential screening, the Benjamini–Hochberg method was used for multiple-testing correction, and the false discovery rate (FDR) was calculated. An adjusted *P* value (Padj) <0.05 was considered statistically significant.

Spearman correlation analysis was used to evaluate the relationships between glycan traits and clinical parameters in CSF. All statistical tests were two-sided, and a $P < 0.05$ was considered statistically significant. It should be noted that the sample sizes in each group were small (DC group, n=3; VM group, n=3; PM group, n=6), resulting in limited statistical power. Therefore, parameters with *P* values between 0.05 and 0.10 were interpreted cautiously as potential trends and were not considered confirmatory evidence of between-group differences.

Results

Clinical Characteristics

A total of 12 pediatric CSF samples were included in this study, comprising a leukemia disease control group (DC, n = 3), a viral meningitis group (VM, n = 3), and a purulent meningitis group (PM, n = 6). The etiological spectrum of pathogens identified in the PM group (n = 6) showed some heterogeneity, including *Pseudomonas aeruginosa* (2 cases), *Staphylococcus aureus* (2 cases), *Escherichia coli* (1 case), and *Streptococcus pneumoniae* (1 case). The clinical and biochemical characteristics of the participants in each group are presented in Table 1.

Table 1 Clinical and biochemical characteristics of the PM, VM, and DC groups[6]

Group		Gender	Age(Year/Month)	CSF WBC(×10⁶/L)	CSF Protein, (g/L)	CSF Glucose, (mmol/L)	CSF Chloride (mmol/l)	Serum PCT, (ng/mL)	LDH-L(U/L)	CK-BB, (U/L)	CRP(mg/ml)
DC (n=3)	C1	Female	2Y3M	0	0.14	3.25	124.7	0.18	344	35	<0.85
	C2	Female	2Y	0	0.17	2.96	124.5	0.18	305	43	<0.85
	C3	Female	2Y	1	0.24	3.82	123.2	0.18	212	25	<0.85
VM (n=3)	V1	Male	3Y2M	156	0.58	3.04	119.3	0.05	519	70	<0.85
	V2	Female	5Y11M	136	0.52	3.41	118.7	0.06	207	16	1.92
	V3	Male	3Y2M	28	0.33	3.54	129.2	0.04	340	63	<0.84
PM (n=6)	P1	Female	7Y10M	1259#	3.38*	3.67	116.6	0.04	198	17	2.19
	P2	Female	1Y1M	1392#	0.75	3.43	118.3	0.08	178	19	14.1

[6] Data were de-identified, patient-level clinical records. H and *P* values were calculated using the Kruskal–Wallis test across the three groups (df = 2). * indicates a significant difference versus the disease control (DC) group ($P < 0.05$), and # indicates a significant difference versus the viral meningitis (VM) group ($P < 0.05$), based on SPSS-adjusted pairwise comparisons.

	P3	Female	2Y7M	43629*#	1.6*	0.04	118.3	13.08	217	20	154
	P4	Male	1Y6M	15240*#	3.98*	2.85	111.8	3.68	307	23	38.9
	P5	Female	10Y5M	252	1.9*	1.67	118.2	0.09	324	19	<0.84
	P6	Male	2Y3M	677	1.27*	5.27	104.5	0.28	319	31	16.9
H		2.75	2.74	9.379	9.346	0.231	8.453	4.238	1.462	3.165	na
p		0.253	0.254	**0.009**	**0.009**	0.891	**0.015**	0.120	0.482	0.205	na

TEM analysis

The vesicles ranged from 20–200 nm in diameter and exhibited a spherical or cup-shaped morphology with a continuous bilayer membrane, indicating the presence of exosome-like vesicles in the CSF of children with meningitis (Fig. 1).

NTA results

The vesicles had a mean diameter of 123.7 nm and a concentration of 6.7×10^12 particles/L(Fig. 2).

Western blot analysis

The extracellular vesicle marker proteins CD9, CD81, and TSG101 were positively expressed, whereas Calnexin expression was negative(Fig. 3).

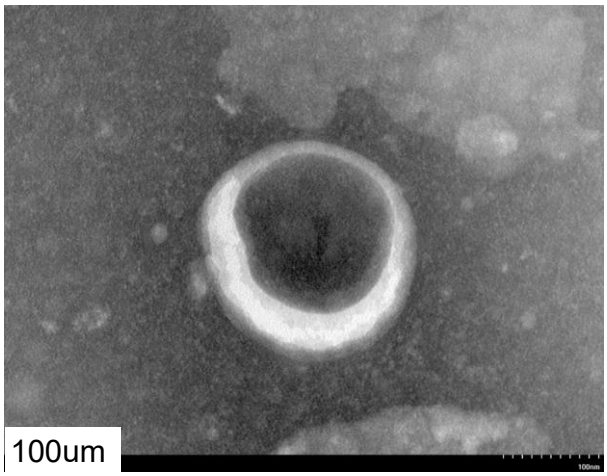


Fig. 1 Exosome morphology observed by transmission electron microscopy

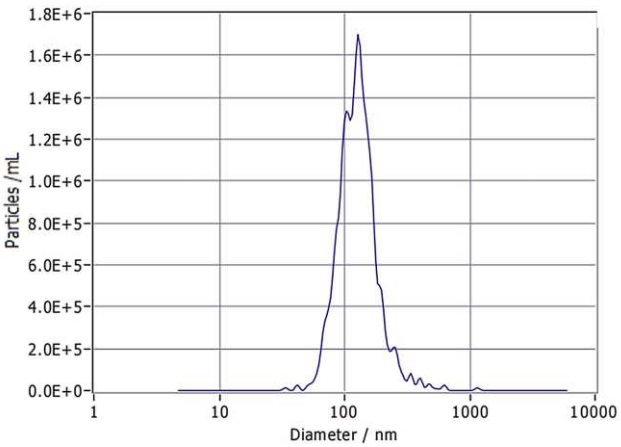


Fig. 2 Nanoparticle tracking analysis

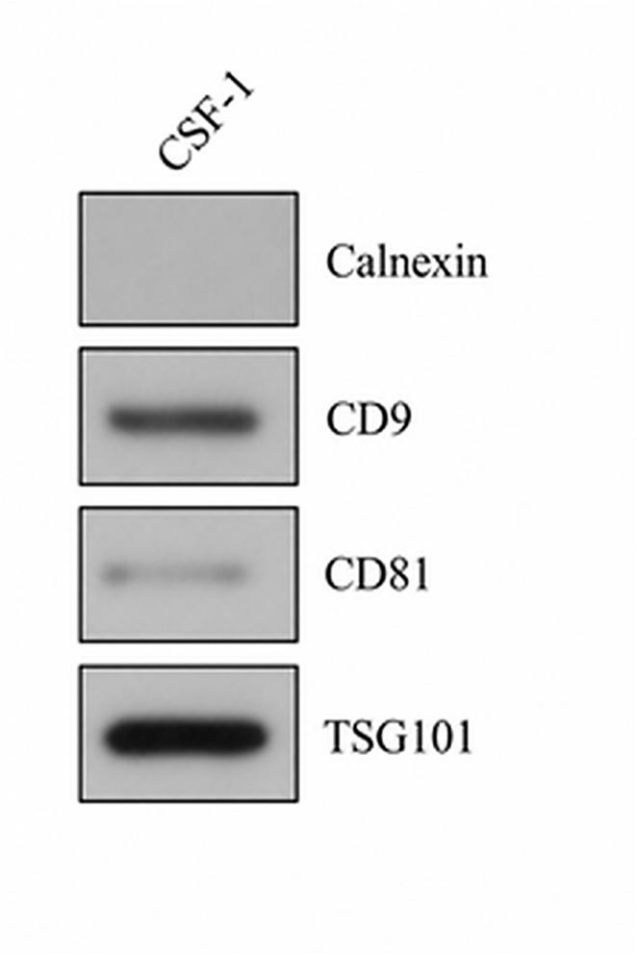
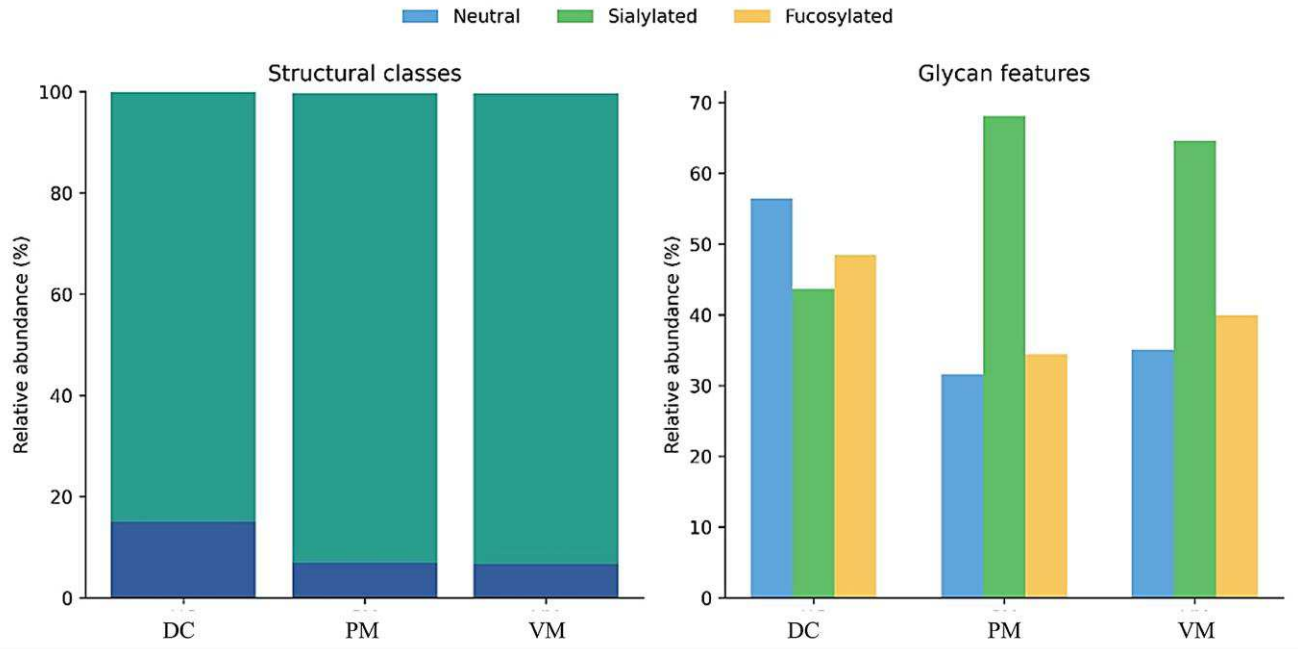


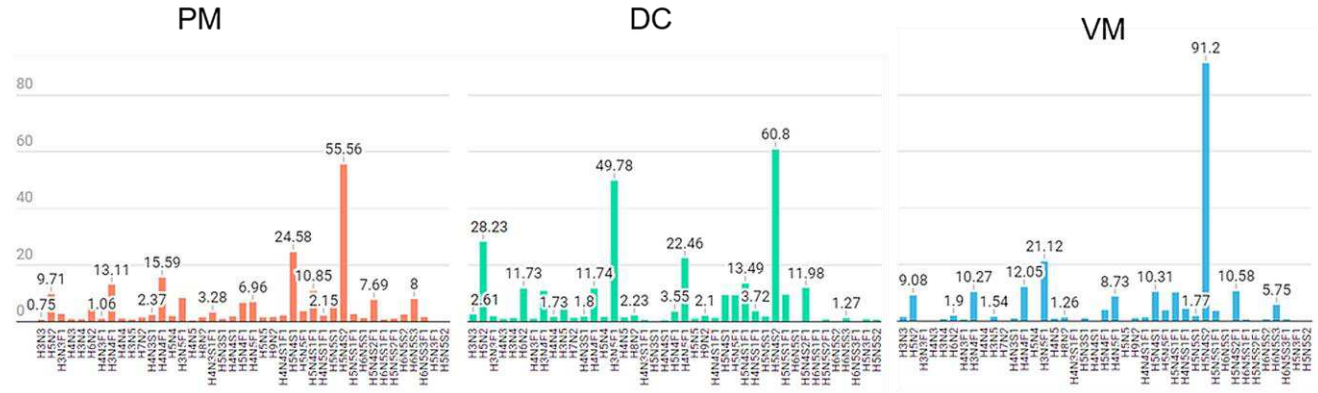
Fig. 3 Western blot assay of the expression of exosome marker proteins CD9、CD81、TSG101.

Comparison of the Relative Abundances of CSF-EV N-Glycans among the DC, VM, and PM Groups

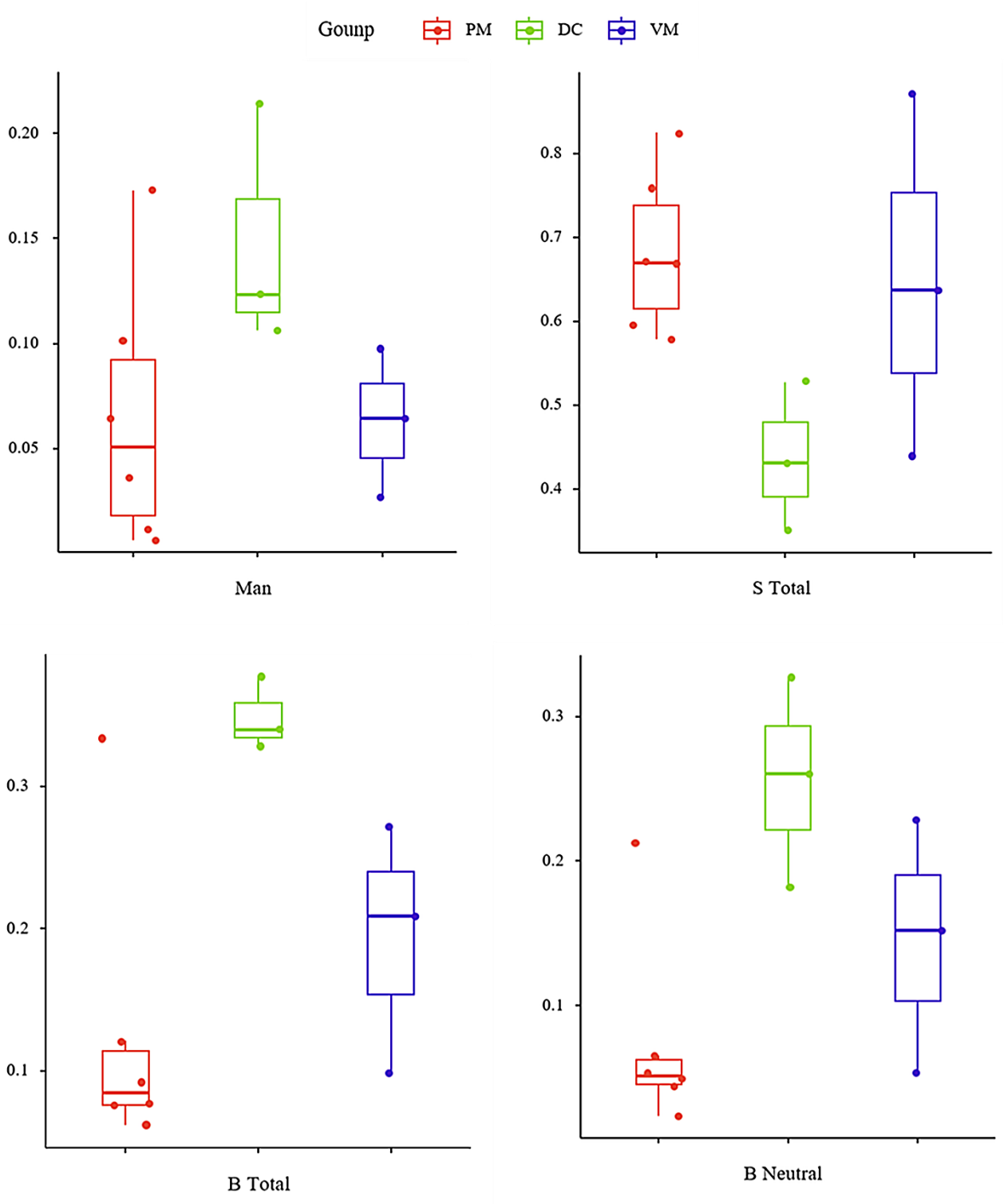
a



b



To assess the overall patterns of N-glycan alterations across groups, we analyzed the relative abundances of structural classes and specific glycan-derived traits in the disease control (DC), purulent meningitis (PM), and viral meningitis (VM) groups (Fig.4). The proportion of neutral



c

Fig. 4 Structural classification, derived glycan traits, and quantitative landscape of CSF N-glycans in a pediatric central nervous system infection cohort

(a) Comparison of the relative abundance of N-glycan structural classes (left, neutral and acidic/sialylated glycans) and derived glycan traits (right, neutral, sialylated, and fucosylated glycans) among the disease control (DC, n = 3), purulent meningitis (PM, n = 6), and viral meningitis (VM, n = 3) groups. (b) Quantitative

distribution of individual N-glycan structures in the DC, PM, and VM groups based on MALDI-TOF-MS measurements. Values above the representative peaks indicate the mean relative abundance (%) of each glycan within the corresponding group. (c) Infection-associated alterations in CSF N-glycan structural features. Representative glycan-derived traits are shown as relative abundance distributions among the DC, PM, and VM groups. Box plots indicate the median and interquartile range, and dots represent individual samples. Kruskal–Wallis tests identified significant differences in B Total (P = 0.0455) and B Neutral (P = 0.0482) among the three groups, whereas S Total (P = 0.0656) and Man (P = 0.1034) showed non-significant trends.

glycans was significantly lower in the PM and VM groups than in the DC group(Fig.4 a). Consistent with previous reports[14], the relative abundance of sialylated glycans was markedly increased in both the PM and VM groups, reaching approximately 68% and 65%, respectively, compared with approximately 44% in the DC group (Fig. 4 b). In contrast, neutral glycans were substantially reduced under pathological conditions, whereas fucosylated glycans also showed a modest decrease in the central nervous system infection groups. These findings indicated that acute central nervous system infection was associated with a marked shift in the CSF N-glycome toward a highly sialylated phenotype.

To further characterize the structural features underlying alterations in CSF N-glycans, multiple glycan-derived traits were calculated based on the identified N-glycans (Fig. 4 c), including bisecting glycans, sialylation, and high-mannose glycans, to evaluate changes in N-glycan structural composition across different infectious states. Among the glycan-derived traits, bisecting N-glycan-related features showed relatively pronounced differences among the three groups. The Kruskal–Wallis test revealed a significant difference in B Total among the DC, VM, and PM groups (P=0.0455). Further analysis showed that B Neutral also differed significantly among the three groups (P=0.0482), suggesting that the observed alterations in bisecting N-glycans were primarily attributable to changes in neutral bisecting structures rather than sialylated bisecting structures. In addition to bisecting structures, sialylation-related traits showed a potential trend toward between-group variation. S Total showed a near-significant difference among the three groups (P=0.0656), suggesting that infection status may be associated with modulation of terminal sialylation of CSF N-glycans. High-mannose N-glycans (Man) also showed a potential trend toward differential distribution among the groups (P=0.1034), suggesting that N-glycan maturation and processing may be influenced by the infection-associated microenvironment[21]. Given the limited sample size, these borderline P values should be regarded as hypothesis-generating findings rather than confirmatory evidence, and their robustness requires validation in larger cohorts.

Clinical Baseline and Biochemical Characteristics of the Retrospective Study Cohort

At the time of lumbar puncture, children in the DC group were confirmed to have no central nervous

system leukemia (CNSL) involvement based on serial cytological assessments and flow cytometry, and none had concomitant active secondary infections. Therefore, the DC group was considered an appropriate reference group representing a post-treatment central nervous system microenvironment without active CNS infection. Key CSF and peripheral inflammatory parameters were statistically compared and visualized across groups (Fig.5) to characterize quantitative differences associated with different infectious states and provide a reference for subsequent correlation analyses between glycomic features and clinical parameters.

Quantitative analysis of key CSF parameters showed that, compared with the uninfected DC baseline, the VM group exhibited significantly higher CSF white blood cell (WBC) counts (Fig. 5A) and CSF protein levels (Fig. 5B) ($P < 0.05$). Although the median CSF WBC count and protein level were numerically higher in the PM group, the differences compared with the DC group did not reach statistical significance ($P > 0.05$, ns). This finding may be attributable to substantial interindividual heterogeneity in disease severity and the timing of clinical presentation within the PM group. For example, the WBC counts and protein levels in two children (P3 and P4) were markedly higher than those in the remaining PM samples **(Table 1)**.

Meanwhile, peripheral inflammatory status, as assessed by serum procalcitonin (PCT) levels (Fig. 5C), did not differ significantly among the three groups ($P > 0.05$, ns). This finding may suggest that, owing to the underlying malignancy and chemotherapy exposure, the peripheral immune system in the DC group may have been in a distinctive baseline state unrelated to active infection. The mechanisms underlying this observation are beyond the scope of the present dataset and warrant further investigation.

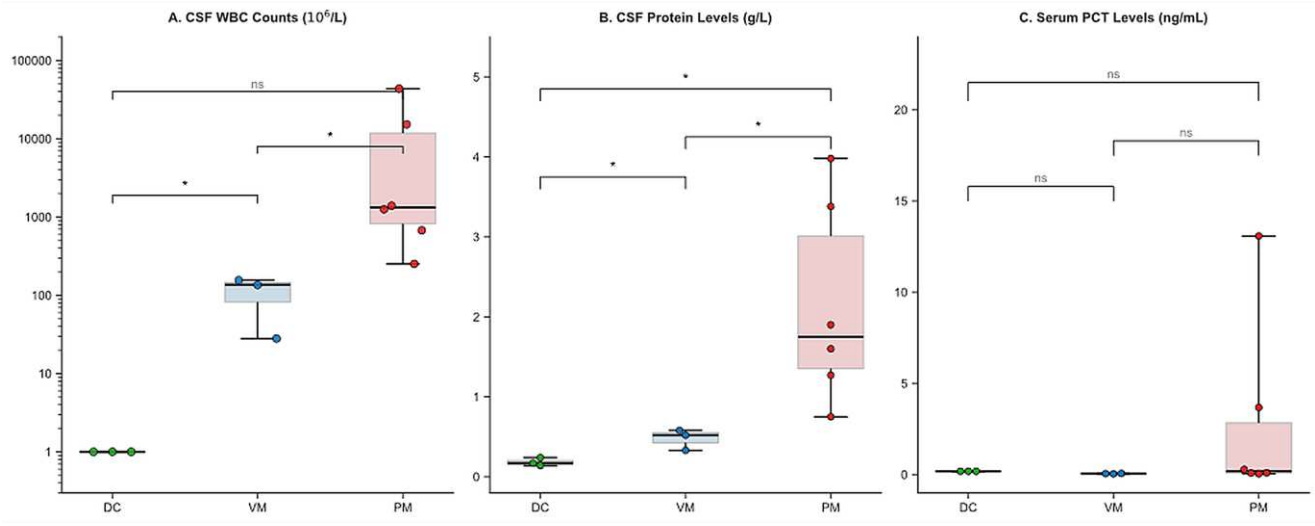


Fig. 5 Comparison of major CSF parameters and serum PCT among DC, VM, and PM. Boxplots represent the distribution of (A) CSF WBC counts, (B) CSF protein levels, and (C) serum PCT levels across the retrospective cohorts. Individual data points are superimposed with jittering. Statistical significance was evaluated by the Kruskal-Wallis test (*$P < 0.05$; ns, non-significant).

Overall CSF N-Glycosylation Profiles and Molecular Subtyping under Different Infectious Exposures

To assess whether acute pathogen invasion substantially disrupted the central glycan homeostasis established during the post-treatment baseline state, unsupervised hierarchical clustering was performed based on the relative abundances of 15 major CSF N-glycan traits (Fig. 6). The unsupervised hierarchical clustering analysis separated the retrospective cohort into three distinct clusters, with the resulting classification broadly concordant with the clinical diagnoses. These findings suggested that CSF-EV N-glycosylation profiles may have potential to discriminate between different pathogen exposure states. However, given the limited sample size (n=12) relative to the feature dimension (15 traits), the clustering results may be susceptible to overfitting, and their discriminatory performance requires validation in larger cohorts.

The overall glycomic profiles showed that the uninfected DC baseline samples (C1–C3) clustered characteristically within a high-abundance region dominated by the basal core glycan framework (G0 Total, G1 Total, G Total, F Neutral, and F Total) and bisecting glycan structures (B Neutral and B Total), which appeared as prominent high-intensity red Z-score bands in the heatmap.

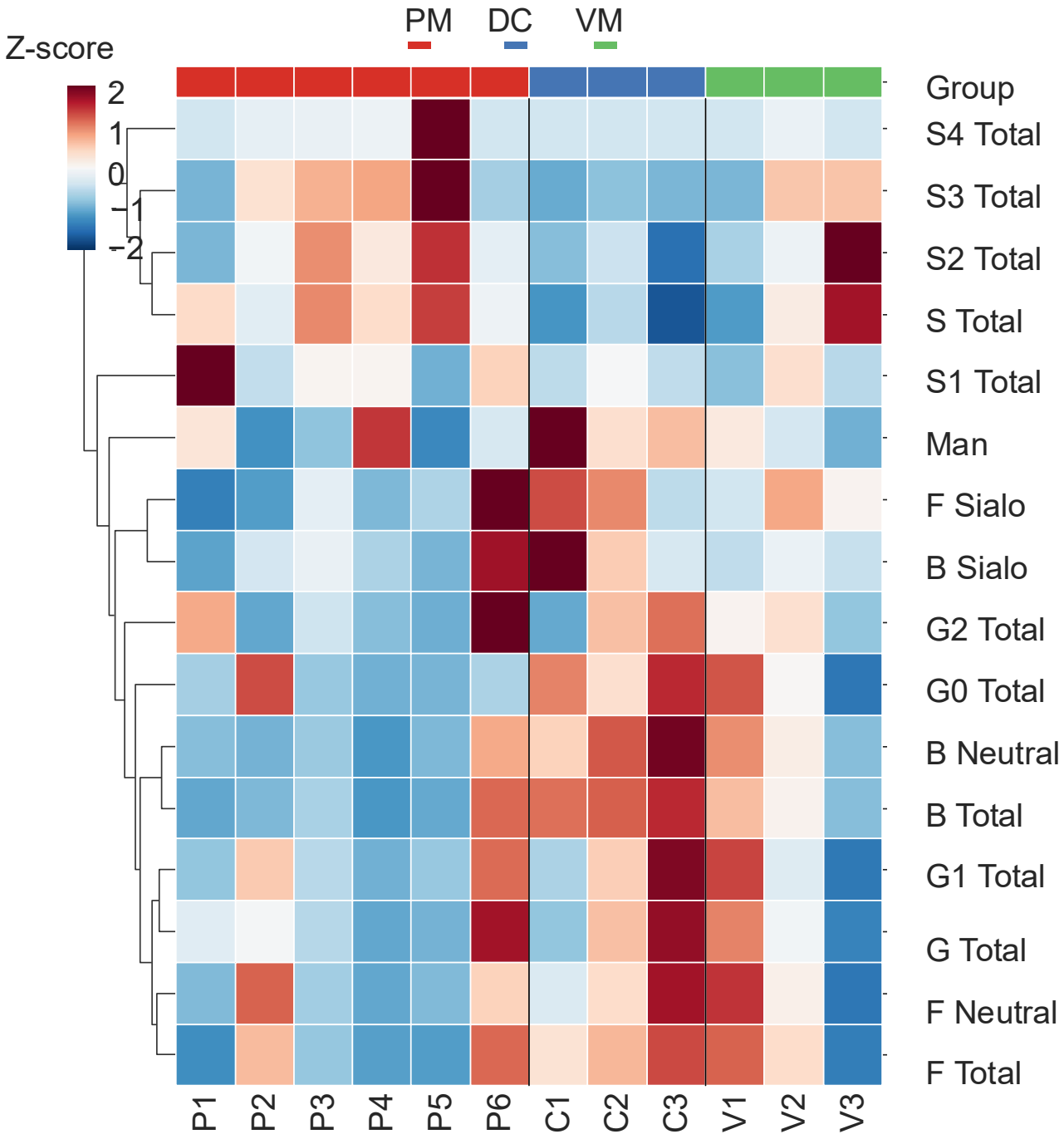


Fig. 6 Hierarchical clustering of 15 major CSF N-glycan traits comparing DC, VM, and PM. Red indicates an increase in Z-score intensity while blue indicates a decrease in Z-score intensity. Columns represent individual retrospective pediatric patients: DC (C1–C3), VM (V1–V3), PM (P1–P6).

Following acute pathogen invasion, this post-treatment pathological homeostasis underwent pronounced and structure-specific remodeling.Purulent meningitis (PM) cluster: The PM cluster exhibited a characteristic molecular shift toward highly antennated, polysialylated complex glycan structures. In particular, S4 Total and S3 Total showed marked enrichment in most PM samples, most

prominently in sample P5. This enrichment was accompanied by a coordinated depletion and downregulation of the basal core glycan framework (G0/G1/G Total) that characterized the DC baseline.Viral meningitis (VM) cluster: The VM cluster displayed a distinctly different molecular profile, characterized primarily by selective increases in disialylated glycans (S2 Total) and total sialylation (S Total), particularly in sample V3. Compared with the PM group, highly antennated polysialylated structures remained at very low abundance in the VM cohort, which also exhibited the most pronounced systemic depletion of basal core glycan structures among the three groups.

Correlation and Regression Analysis of CSF Glycosylation Traits and Central Clinical Parameters

Having established characteristic molecular patterns of CSF-EV glycomic profiles across different infectious states, we further investigated whether these glycan alterations were quantitatively associated with the actual inflammatory status of the children. Spearman correlation analysis was performed between eight core glycan traits and the available continuous clinical variables in the cohort (Fig. 7A). The correlation analysis revealed a significant positive association between total bisecting GlcNAc (B_Total) and peripheral serum procalcitonin (PCT) levels ($r > 0.5$, $P < 0.05$), whereas none of the other glycan traits examined, including Man, G0/G1/G2/G Total, F Total, F Neutral, and S Total, showed statistically significant correlations with any of the available central or peripheral routine clinical parameters[29].

An XY linear regression model (Fig. 7B) further quantitatively confirmed a strong positive association between peripheral serum PCT levels and the relative abundance of B_Total in CSF (regression coefficient $r = 0.681$, $P = 0.015$). Inspection of the retrospective scatterplot distribution showed that some disease control samples without meningitis (DC group, designated as the N Group in the Fig.7) exhibited relatively high peripheral PCT levels together with increased CSF B_Total abundance.

Because the DC group comprised children with leukemia in remission, their underlying disease status and previous treatment history may have influenced systemic glycosylation homeostasis. Previous studies have shown that patients with hematological malignancies may exhibit altered serum protein N-glycan profiles, suggesting that tumor-associated pathological states may contribute to the regulation of the systemic glycosylation environment[34]. In addition, clinical interventions, including chemotherapy and other systemic treatments, may induce dynamic remodeling of the serum N-glycome. Therefore, the enrichment of B_Total observed in the DC group may partly reflect glycosylation characteristics associated with the underlying disease or previous treatment exposure rather than infection status alone.

During acute central nervous system infection, as observed in the PM and VM groups, this potential baseline homeostasis may be influenced by infection-associated inflammatory responses, resulting in further remodeling of the CSF N-glycome and alterations in the distribution pattern of B_Total. However,

because the present study did not stratify the effects of treatment regimens, chemotherapy timing, or disease remission status on glycosylation profiles, the dynamic changes in B_Total across different clinical states and its specific regulatory relationship with the infectious process require further validation in larger prospective cohorts.

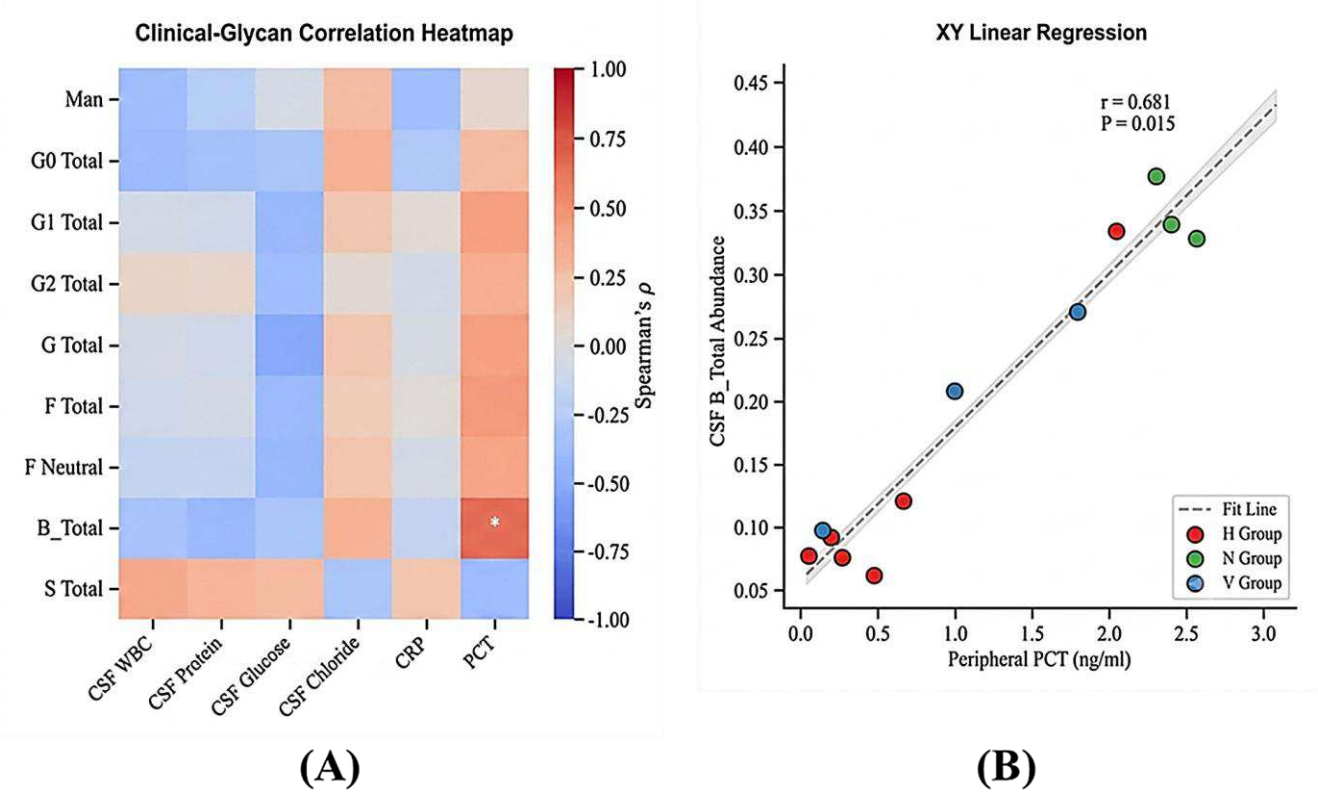


Fig. 7. Correlation matrix and linear regression modeling between CSF glycan traits and clinical markers. (A) Spearman correlation heatmap between 8 key CSF glycan traits and major clinical continuous parameters, with asterisks (*) indicating statistical significance ($P < 0.05$). (B) XY linear regression analysis between peripheral serum PCT levels and CSF B_Total relative abundance ($r = 0.681$, $P = 0.015$).”H Group"(PM)、"N Group"(DC)、"V Group"(VM).

Conclusions and future directions

Children with meningitis were found to have extracellular vesicles in the CSF, consistent with previous findings in adult CSF studies. Transmission electron microscopy (TEM) confirmed that the vesicles exhibited typical cup-shaped or spherical morphology with intact bilayer membranes. Nanoparticle tracking analysis (NTA) further demonstrated that the vesicles were predominantly distributed within the typical physical size range of exosomes (50–200 nm), with a median particle diameter (X50) of 123.7 nm and a heterogeneous distribution characterized by a single dominant peak. Western blot analysis showed strong and consistent expression of the transmembrane proteins CD9 and CD81 and the endosomal sorting complex-associated protein TSG101, whereas the endoplasmic reticulum contamination marker Calnexin was completely absent. Collectively, these comprehensive

methodological characterizations were highly consistent with previous reports describing extracellular vesicle characterization in adult CSF and neurological disease cohorts[27].

High-resolution matrix-assisted laser desorption/ionization time-of-flight mass spectrometry (MALDI-TOF-MS) enabled precise quantification of differences in N-glycan profiles between CSF samples from patients with central nervous system infections and controls. Multiple infection-associated alterations in N-glycosylation were identified, including quantitative changes in glycan class distributions, such as a trend toward differences in high-mannose glycans, suggesting that N-glycan maturation and processing may be influenced by infection status, as well as alterations in key structural features of complex N-glycans, including bisecting GlcNAc modification, multiantennary sialylation, galactosylation, and fucosylation.

Importantly, CSF N-glycan profiles showed potential for distinguishing patients with central nervous system infections from controls and, potentially, for discriminating between different types of pathogen infection. This observation was further supported by unsupervised hierarchical clustering analysis. Previous glycomic studies of infectious diseases have demonstrated that unsupervised hierarchical clustering based on serum N-glycan profiles can effectively reveal molecular stratification patterns among patients with different infectious states, providing a rationale for using glycan features for disease subtype classification[34]. These findings suggest that CSF-EV N-glycan profiles may possess discriminatory potential across different infectious states; however, as noted above, this observation remains subject to validation because of the limited sample size. The PM group exhibited pronounced enrichment of highly antennary polysialylated complex structures in the CSF, whereas the VM group showed a characteristic increase in disialylated structures. In contrast, the disease control group was characterized by relatively high abundance of bisecting glycan structures.

Notably, substantial interindividual variability was observed in CSF WBC counts and protein levels within the PM group. In addition to differences in disease severity, this variability may partly have been related to empirical antibiotic treatment administered to some children before diagnostic lumbar puncture. This represents a common clinical confounder in retrospective studies. However, the precise timing of antibiotic administration was not systematically recorded in the present study, precluding direct evaluation of this hypothesis.

Among the two types of central nervous system infections investigated, the PM group exhibited the most pronounced abnormalities in the N-glycan profile. CSF from children with PM was characterized by enrichment of highly antennary polysialylated structures (S3 Total and S4 Total), accompanied by systematic downregulation of the basal core glycan framework. Based on previous studies of neuroinfection and immunological mechanisms[30], it can be hypothesized that bacterial invasion strongly stimulates CNS-infiltrating microglia and astrocytes, together with large numbers of recruited neutrophils, which is consistent with the significantly elevated CSF WBC counts observed in the PM group in the present study, thereby potentially increasing local sialyltransferase activity[31]. Previous

studies have suggested that terminal polysialylated residues may participate in limiting excessive complement activation through interactions with complement regulatory factors[30, 32]. Sialic acid–Siglec interactions are known to participate in immune regulation[36]. Whether the increased sialylated glycan features observed in CSF-EVs directly engage this pathway in pediatric meningitis remains unknown.The enrichment of polysialylated features (S3 Total and S4 Total) on CSF-EVs in the PM group may therefore be related to such protective regulatory mechanisms. However, this interpretation remains speculative and requires direct validation through functional studies, such as complement activity assays and Siglec-binding experiments.

In contrast, the VM group exhibited a distinctly different molecular profile and remodeling pattern. Samples from patients with VM primarily showed a modest increase in disialylation (S2 Total), whereas the basal core glycan framework (G0 Total, G1 Total, G Total, F Neutral, and F Total) showed systematic depletion and downregulation. Viral infection may induce endoplasmic reticulum stress (ER stress) in endothelial cells and neurons and interfere with the normal function of key Golgi glycan-processing enzymes, such as galactosyltransferases and fucosyltransferases. This mechanism may represent one potential explanation for the marked downregulation of the basal core glycan framework (G0/G1/G Total, F Neutral, and F Total) observed in the VM group. Previous studies have also suggested that reduced core glycosylation may be associated with impaired stability of tight junction proteins at the blood–brain barrier, which could partly explain the elevated CSF protein levels observed in children with VM[29]. However, tight junction proteins and ER stress-related markers were not directly measured in the present study; therefore, this interpretation remains speculative and requires confirmation in future mechanistic studies.

Bisecting glycan structures (B Neutral and B Total) remained relatively abundant in the DC group but were significantly reduced in both the PM and VM groups, suggesting that this alteration may be associated with infection status itself rather than being specific to a particular type of infection. Previous studies have reported that bisecting structures generated by MGAT3-mediated glycosylation exert steric effects that restrict further extension and modification of glycan termini, thereby functioning as a form of “rate-limiting” regulatory mechanism[20,34]. We therefore hypothesize that children in the DC group, whose immune homeostasis may have been influenced by their underlying disease and chemotherapy exposure, maintained relatively high levels of bisecting glycan modification. Upon acute CNS infection, increased demands for terminal sialylation and highly antennary structures during the immune response may lead to downregulation of this rate-limiting mechanism, thereby shifting glycan processing toward complex and polysialylated structures. This hypothesis is directionally consistent with the positive correlation between B_Total and serum PCT observed in the present study (Fig. 7), but direct validation, such as measurement of MGAT3 expression, is required.

Several limitations of this study should be considered when interpreting the findings. First, the sample size was small (DC group n=3, VM group n=3, PM group n=6), resulting in limited statistical

power. Accordingly, parameters with P values between 0.05 and 0.10 should be interpreted as potential trends rather than confirmatory differences, and these findings require validation in larger cohorts.

Notably, the proportion of Pseudomonas aeruginosa infections in the PM group was relatively high (2/6), differing from the typical epidemiological profile of community-acquired bacterial meningitis in children, in which Streptococcus pneumoniae, Neisseria meningitidis, and Haemophilus influenzae are the predominant pathogens[37]. This discrepancy may be related to the fact that all participants were recruited from a tertiary pediatric hospital and that some children had underlying diseases or previous healthcare exposure. Previous studies have shown that Pseudomonas aeruginosa meningitis occurs more frequently in healthcare-associated infections, following neurosurgical procedures, or in immunocompromised patients[37]. Because of the limited sample size and the absence of pathogen-stratified analyses, whether glycosylation remodeling differs specifically according to the causative pathogen remains to be determined in larger studies.

Consistent with previous reports[38], the local alterations in CSF glycosylation observed in this study may be temporally or spatially dissociated from inflammatory markers measured in peripheral blood. Furthermore, because this was a retrospective study, some children in the PM group may have received empirical antibiotic treatment before diagnostic lumbar puncture. This may have contributed to the substantial within-group variability in CSF WBC counts and protein levels and to the lack of statistically significant differences compared with the DC group. However, because the timing of antibiotic administration was not systematically recorded, sensitivity analysis could not be performed to assess this potential confounding effect.

Given the limited sample size and exploratory nature of the study, diagnostic performance analyses, including receiver operating characteristic (ROC) curves, area under the curve (AUC), sensitivity, and specificity, were not performed for the differential glycan traits. In addition, the mechanistic hypotheses proposed in the Discussion were not directly validated using functional experiments, such as MGAT3 expression analysis, complement activity assays, or Siglec-binding experiments.

In summary, this exploratory study provides preliminary evidence that central nervous system infection may be accompanied by characteristic remodeling of CSF-EV N-glycosylation, with distinguishable remodeling patterns across different types of pathogen infection. Quantitative glycan-trait profiling based on high-resolution mass spectrometry (MALDI-TOF-MS) provides a new molecular perspective and hypothesis-generating framework for the differential diagnosis of bacterial and viral central nervous system infections in children. The clinical utility of these glycomic features remains to be validated in larger cohorts.

Compliance with Ethical Standards

Competing interests The authors declare no competing interests.

Funding 2025 Hubei Provincial Natural Science Foundation Innovation and Development Joint Fund Project (2025AFD478,

2025AFD523),2025–2026 Youth Project of the Scientific Research Program of Traditional Chinese Medicine, Hubei Provincial Administration of Traditional Chinese Medicine (ZY2025Q008)

Ethics approval The study was approved by the Medical Ethics Committee of Wuhan Children's Hospital (approval No. 2024R053-R01), and written informed consent was obtained from the guardians of all participants.

Data availability They are provided as required.

S1 The individual glycoforms of CSF with the same glycan features were grouped and the percentage was calculated by the formula.[7]

Trait	Description	Formula
Man	Percentage of mannosylated structures in total CSF glycans	(peak2+peak6+peak8+peak12+peak20+peak27) / (total peaks)
G0 Total	Percentage of agalactosylated structures in total CSF glycans	(peak1+peak3+peak5+peak8+peak9+peak11+peak18) / (total peaks)
G1 Total	Percentage of mono-galactosylated structures in total CSF glycans	(peak4+peak7+peak10+peak15+peak16+peak19+peak25) / (total peaks)
G2 Total	Percentage of di-galactosylated structures in total CSF glycans	(peak17+peak24+peak26+peak32) / (total peaks)
G Total	Percentage of galactosylated structures in total CSF glycans	(peak4+peak7+peak10+peak15+peak16+peak17+peak19+peak24+peak25+peak26+peak32+peak33) / (total peaks)
F Neutral	Percentage of neutral fucosylated	(peak3+peak7+peak9+peak16+peak18+peak24+peak25+peak32) / (total peaks)

[7] Glycan-derived traits were calculated according to established structural classification principles. Glycan structures were annotated by comparison with publicly available glycan reference resources, including GlycoStore, and the assignment of individual glycan peaks to specific derived traits was performed according to their annotated structural features.

	structures in total CSF glycans	
F Sialo	Percentage of sialylated structures of fucosylation in total CSF glycans	(peak20+ peak29+ peak34+peak35+peak38+peak40+ peak42+peak43+peak46+peak49+peak50+peak52+peak54) / (total peaks)
F Total	Percentage of structures with core-fucose in total CSF glycans	(peak3+peak7+peak9+ peak14+peak16+peak18+ peak21+peak24+peak25+peak29+peak32+peak34+peak35+peak38+peak40+peak42+peak43+peak46+peak49+peak50+peak52+peak54) / (total peaks)
B Neutral	Percentage of neutral bisected structures in total CSF glycans	(peak11+peak18+peak25+peak26+peak32) / (total peaks)
B Sialo	Percentage of sialyted structures with bisecting GlcNAc in total CSF glycans	(peak31+peak35+peak36+peak38+peak41+peak43 / (total peaks)
B Total	Percentage of bisected structures in total CSF glycans	(peak11+peak18+peak25+peak26+peak31+peak32+peak35+peak36+peak38+peak41+peak43) / (total peaks)
S1 Total	Percentage of mono-sialylated structures in total CSF glycans	(peak13+peak21+peak22+peak23+peak28+peak29+peak30+peak31+peak34+peak35+peak36+peak38+peak39+peak42+peak45) / (total peaks)
S2 Total	Percentage of di-sialylated structures in total CSF glycans	(peak37+peak40+peak41+peak43+peak44+peak46+peak48+peak50) / (total peaks)
S3 total	Percentage of tri-sialylated structures in total CSF glycans	(peak47+peak49+peak51+peak52) / (total peaks)

S4 total	Percentage of tetra-sialylated structures in total CSF glycans	(peak53+peak54) / (total peaks)
S Total	Percentage of sialylated structures in total CSF glycans	(peak13+peak21+peak22+peak23+peak28+peak29+peak30+peak31+peak34+peak35+peak36+peak37+peak38+peak39+peak40+peak41+peak42+peak43+peak44+peak45+peak46+peak47+peak48+peak49+peak50 +peak51+peak52+ peak53+peak54) / (total peaks)

Reference

[1] Lucas, M.J., Brouwer, M.C., van de Beek, D.: Neurological sequelae of bacterial meningitis. J. Infect. 73, 18–27 (2016). https://doi.org/10.1016/j.jinf.2016.04.009

[2] van de Beek, D., Cabellos, C., Dzupova, O., et al.: ESCMID guideline: diagnosis and treatment of acute bacterial meningitis. Clin. Microbiol. Infect. 22 Suppl 3, S37–S62 (2016). https://doi.org/10.1016/j.cmi.2016.01.007

[3] Lee, B.R., Sasidharan, A., Harrison, C.J., Selvarangan, R.: Positive impact of routine testing for enteroviruses and parechovirus on length of hospitalization and antimicrobial use among inpatients ≤6 months of age. J. Clin. Microbiol. 59, e02106-20 (2020). https://doi.org/10.1128/JCM.02106-20

[4] Duong, Q.A., Pittet, L.F., Curtis, N., Zimmermann, P.: Antibiotic exposure and adverse long-term health outcomes in children: a systematic review and meta-analysis. J. Infect. 85, 213–300 (2022). https://doi.org/10.1016/j.jinf.2022.01.005

[5] Shen, Y., Zhang, J., Zhao, X., et al.: Blood procalcitonin level as a diagnostic marker of pediatric bacterial meningitis: a systematic review and meta-analysis. Front. Pediatr. 9, 665881 (2021). https://doi.org/10.3389/fped.2021.665881

[6] Henry, B.M., Roy, J., Ramakrishnan, P.K., et al.: Procalcitonin as a serum biomarker for differentiation of bacterial meningitis from viral meningitis in children: evidence from a meta-analysis. Clin. Pediatr. (Phila.) 55, 749–764 (2016). https://doi.org/10.1177/0009922815606414

[7] Dubos, F., Korczowski, B., Aygun, D.A., et al.: Serum procalcitonin level and other biological markers to distinguish between bacterial and aseptic meningitis in children: a European multicenter case cohort study. Arch. Pediatr. Adolesc. Med. 162, 1157–1163 (2008). https://doi.org/10.1001/archpedi.162.12.1157

[8] Santos, K.T.D.J., Layug, E.J.V., Calotes-Castillo, L.V., et al.: The diagnostic utility of cerebrospinal fluid procalcitonin for acute bacterial meningitis and ventriculitis in children: a multicenter prospective study. Acta Med. Philipp. 59, 33–43 (2025). https://doi.org/10.47895/amp.v59i13.11218

[9] Ivaska L, Herberg J, Sadarangani M. Distinguishing community-acquired bacterial and viral meningitis: Microbes and biomarkers. J Infect. 88(3), 106111 (2024). https://doi.org/10.1016/j.jinf.2024.01.010

[10] Mathieu, M., Martin-Jaular, L., Lavieu, G., Théry, C.: Specificities of secretion and uptake of exosomes

and other extracellular vesicles for cell-to-cell communication. Nat. Cell Biol. 21, 9–17 (2019). https://doi.org/10.1038/s41556-018-0250-9

[11] Lotfy, A., AboQuella, N.M., Wang, H.: Mesenchymal stromal/stem cell (MSC)-derived exosomes in clinical trials. Stem Cell Res. Ther. 14, 66 (2023). https://doi.org/10.1186/s13287-023-03287-7

[12] Théry, C., Witwer, K.W., Aikawa, E., et al.: Minimal information for studies of extracellular vesicles 2018 (MISEV2018): position statement of the International Society for Extracellular Vesicles and update of the MISEV2014 guidelines. J. Extracell. Vesicles 7, 1535750 (2018). https://doi.org/10.1080/20013078.2018.1535750

[13] Li S, Li W, Wu X, Zhang B, Liu L, Yin L. Immune cell-derived extracellular vesicles for precision therapy of inflammatory-related diseases. J Control Release. 368, 533–547 (2024). https://doi.org/10.1016/j.jconrel.2024.03.007

[14] Street JM, Barran PE, Mackay CL, et al. Identification and proteomic profiling of exosomes in human cerebrospinal fluid. J Transl Med. 10, 5 (2012). https://doi.org/10.1186/1479-5876-10-5

[15] Williams, C., Royo, F., Aizpurua-Olaizola, O., et al.: Glycosylation of extracellular vesicles: current knowledge, tools and clinical perspectives. J. Extracell. Vesicles 7, 1442985 (2018). https://doi.org/10.1080/20013078.2018.1442985

[16] Vrablova, V., Kosutova, N., Blsakova, A., et al.: Glycosylation in extracellular vesicles: isolation, characterization, composition, analysis and clinical applications. Biotechnol. Adv. 67, 108196 (2023). https://doi.org/10.1016/j.biotechadv.2023.108196

[17] Li, Y., Wang, J., Chen, W., Lu, H., Zhang, Y.: Comprehensive review of MS-based studies on N-glycoproteome and N-glycome of extracellular vesicles. Proteomics 24, e2300065 (2024). https://doi.org/10.1002/pmic.202300065

[18] Groux-Degroote, S., Cavdarli, S., Uchimura, K., Allain, F., Delannoy, P.: Glycosylation changes in inflammatory diseases. Adv. Protein Chem. Struct. Biol. 119, 111–156 (2020). https://doi.org/10.1016/bs.apcsb.2019.08.008

[19] Nagae, M., Yamaguchi, Y., Taniguchi, N., Kizuka, Y.: 3D structure and function of glycosyltransferases involved in N-glycan maturation. Int. J. Mol. Sci. 21, 437 (2020). https://doi.org/10.3390/ijms21020437

[20] Radovani, B., Gudelj, I.: N-Glycosylation and inflammation: the not-so-sweet relation. Front. Immunol. 13, 893365 (2022). https://doi.org/10.3389/fimmu.2022.893365

[21] van Kooyk, Y., Rabinovich, G.A.: Protein-glycan interactions in the control of innate and adaptive immune responses. Nat. Immunol. 9, 593–601 (2008). https://doi.org/10.1038/ni.f.203

[22] Čaval, T., Heck, A.J.R., Wuhrer, M., et al.: High-resolution mass spectrometry captures glycan isomer heterogeneity in clinical CSF samples. Anal. Bioanal. Chem. 414, 1589–1601 (2022). https://doi.org/10.1007/s00216-021-03781-w

[23] Haukedal, H., Freude, K.K.: Implications of glycosylation in Alzheimer's disease. Front. Neurosci. 14, 625348 (2021). https://doi.org/10.3389/fnins.2020.625348

[24] Harvey, D.J.: Analysis of carbohydrates and glycoconjugates by matrix-assisted laser desorption/ionizatio n mass spectrometry: an update for 2019–2020. Mass Spectrom. Rev. 42, 1984–2206 (2023). https://doi.org/1 0.1002/mas.21806

[25] Messina, A., Romeo, D.A., Barone, R., Sturiale, L., Palmigiano, A., Zappia, M., Garozzo, D.: CSF N-Gl ycomics Using MALDI MS Techniques. Methods Mol. Biol. 2785, 49–65 (2024). https://doi.org/10.1007/978-1-0716-3774-6_4

[26] Jeong, H.J., Kim, Y.G., Yang, Y.H., Kim, B.G.: High-throughput quantitative analysis of total N-glycans by matrix-assisted laser desorption/ionization time-of-flight mass spectrometry. Anal. Chem. 84, 3453–3460 (2012). https://doi.org/10.1021/ac203440c

[27] Gornik, O., Lauc, G.: Glycosylation of serum proteins in inflammatory diseases. Dis. Markers 25, 267–2 78 (2008).

[28] Witwer, K.W., Buzás, E.I., Bemis, L.T., et al.: Standardization of sample collection, isolation and analysi s of extracellular vesicles in secretion. J. Extracell. Vesicles 2, 20360 (2013). https://doi.org/10.3402/jev.v2i0. 20360

[29] Shi, S.M., Suh, R.J., Shon, D.J. et al. Glycocalyx dysregulation impairs blood–brain barrier in ageing an d disease. Nature 639, 985–994 (2025). https://doi.org/10.1038/s41586-025-08589-9

[30] Kiermaier, E., Moussion, C., Vaahtomeri, K., et al.: Sialic acid modification of the central extracellular matrix DCs complement activation during meningitis. Acta Neuropathol. 141, 389–405 (2021). https://doi.org/ 10.1007/s00401-020-02256-z

[31] Kizuka, Y., Kitazume, S., Taniguchi, N., et al.: Bisecting GlcNAc: A key regulator of glycan branching and terminal modifications in neurological diseases. Glycoconj. J. 38, 315–323 (2021). https://doi.org/10.1007 /s10719-021-09984-y

[32] Blaum, B.S., Deimling, S., Schmidt, H., et al.: Structural basis of complement factor H activation by ter minal sialic acid patterns. Nat Commun. 13, 1245 (2022). https://doi.org/10.1038/s41467-022-28869-4

[33] Chatterjee, S., Kawahara, R., et al.: Serum N-Glycomics Stratifies Bacteremic Patients Infected with Diff erent Pathogens. J. Clin. Med. 10, 516 (2021). https://doi.org/10.3390/jcm10030516

[34] Reily, C., Stewart, T.J., Renfrow, M.B., Novak, J.: Glycosylation in health and disease. Nat. Rev. Nephr ol. 15, 346–366 (2019). https://doi.org/10.1038/s41581-019-0129-4

[35] Wang, X., Varki, A.: Sialic acid-binding immunoglobulin-like lectins (Siglecs): from molecules to therapi es. Trends Pharmacol. Sci. 24, 488–493 (2003). https://doi.org/10.1016/j.tips.2003.08.002

[36] Oordt-Speets, A.M., Bolijn, R., van Hoorn, R.C., Bhavsar, A., Kyaw, M.H.: Global etiology of bacterial meningitis: A systematic review and meta-analysis. PLoS One. 13, e0198772 (2018). https://doi.org/10.1371/j ournal.pone.0198772

[37] Wang, K.W., Chang, W.N., Huang, C.R., Tsai, N.W., Tsui, H.W., Wang, H.C., Su, T.M., Rau, C.S., Che ng, B.C., Chang, C.S., Chuang, Y.C., Liliang, P.C., Tsai, Y.D., Lu, C.H.: Post-neurosurgical nosocomial bact erial meningitis in adults: microbiology, clinical features, and outcomes. J. Clin. Neurosci. 12, 647–650 (200

5). https://doi.org/10.1016/j.jocn.2004.09.017

[38] Gigase, F.A.J., Smith, E., Collins, B., Moore, K., Snijders, G.J.L.J., Katz, D., Bergink, V., Perez-Rodriquez, M.M., De Witte, L.D.: The association between inflammatory markers in blood and cerebrospinal fluid: a systematic review and meta-analysis. Mol. Psychiatry 28, 1502–1515 (2023). https://doi.org/10.1038/s41380-023-01976-6